arXiv:cond-mat/0602666v3 [cond-mat.dis-nn] 30 Nov 2006

Statics and dynamics of the Lebwohl-Lasher model in the Bethe approximation

N.S. Skantzos [1]

Instituut voor Theoretische Fysica, Celestijnenlaan 200D, Katholieke Universiteit Leuven, B-3001, Belgium

and

J.P.L. Hatchett [2]

† *Hymans Robertson LLP, One London Wall, London EC2Y 5EA, UK*

Abstract

We study the Lebwohl-Lasher model for systems in which spin are arranged on random graph lattices. At equilibrium our analysis follows the theory of spin-systems on random graphs which allows us to derive exact bifurcation conditions for the phase diagram. We also study the dynamics of this model using a variant of the dynamical replica theory. Our results are tested against simulations.

PACS : 89.75.-k, 75.10.Nr, 64.70.Md

1 Introduction

Some physical systems are known to exhibit remarkably sharp, and yet continuous, transitions between the ordered and paramagnetic phase. The most prominent example of these are liquid crystals, systems which combine order like that found in solids with fluidity like that of liquids. Liquid crystals, generally modeled as

[1] nikos@itf.fys.kuleuven.be
[2] jon.hatchett@hymans.co.uk

systems of 'hard-rods', typically exhibit a transition between a phase with no orientational or translational order and a phase where an ordered structure appears. The nature of this transition (continuous vs discontinuous) is an important aspect in practical applications.

One of the most successful models that is able to capture the main characteristics of this transition was introduced by Lebwohl and Lasher in 1973 [1]. In this model the microscopic degrees of freedom ϕ_i take real values in the interval $[0, 2\pi)$, representing the orientation of rod i relative to some fixed reference point. To model the sharp transition, the coupling energy between any pair of rods is taken to have the shape of a deep and narrow well. This energy is taken to be $\epsilon_{ij}(\phi_i - \phi_j) = -JL_p\left(\cos(\phi_i - \phi_j)\right)$ for any pair of rods (i, j) where J represents the strength of the interaction and the function $L_p(x)$ denotes a p-th order Legendre polynomial. In the context of 'hard-rods', p is taken to be even to enforce invariance of the energy ϵ_{ij} under the transformation $\phi \to \phi + \pi$. The value of p plays a crucial role in the nature of the phase transition [2,3]. Generally, this model has been the subject of a significant amount of research (see for instance [2–9] and references therein).

In this paper we study the Lebwohl-Lasher model on a sparse graph motivated both by the interesting nature of the transition and the relative scarcity of analytic results. Our approach can be viewed as the Bethe approximation to the finite dimensional problem, whereby for every site there is an explicit local neighborhood. At equilibrium our analysis follows the finite connectivity (as opposed to fully-connected mean field) theory [10] as developed for real-valued spin systems [11,12]. In the thermodynamic limit we are able to solve this model exactly and derive expressions describing the bifurcation lines in the phase diagram. Numerical evaluation of the order parameters agrees well with the results of the bifurcation analysis and shows that the phase transition, although sharp, is second-order. Comparison of the above analytic results with simulation (Langevin) expreriments shows excellent agreement.

We have also studied the dynamics of this model. Here, in contrast to the thermodynamic analysis which follows a well-studied framework, the terrain of the finite-connectivity dynamics is much less explored. Some recent advances are the papers [13–15]. In the present study we have chosen to extend the results of [13] in order to account for the continuous nature of the spin variables. As in the dynamical replica theory of [16] on which our analysis is based, we arrived at closed equations by assuming equipartitioning of the microscopic state probability within the observable subshells. The resulting analytic description is in good agreement with Langevin simulation for small and very large times, but not sufficiently accu-

rate for intermediate times. This is an artifact of the equipartitioning ansatz and the truncation of the set of observables to a relatively small (and computationally tractable) set.

2 Model Definitions

The model consists of N microscopic variables $\boldsymbol{\phi} = (\phi_1, \ldots, \phi_N)$ representing the angular phase of oscillators relative to a fixed frame of reference. At equilibrium the system is described by the Hamiltonian

$$H(\boldsymbol{\phi}) = -J \sum_{(i,j)\in\mathcal{G}_N} L_p\left(\cos(\phi_i - \phi_j - \omega_{ij})\right) \tag{1}$$

where $\mathcal{G}_N = (\mathcal{V}_N, \mathcal{E}_N)$ denotes a graph instance of a set of vertices $\mathcal{V}_N = \{1, \ldots, N\}$ and edges $\mathcal{E}_N = \{(i,j)|i,j \in \mathcal{V}_N\}$. The function $L_p(x)$ denotes a p-th order Legendre polynomial. The thermal variables take values from the interval $\phi_i \in [0, 2\pi)$ for all $i = 1, \ldots, N$. We also introduced the 'disorder' angle variables $\omega_{ij} \in [0, 2\pi)$ which represent locally preferred orientations between sites i and j. In a physical scenario these are induced by the presence of impurities, cavities, or other heterogeneities. We will assume that the distribution of these variables is for all $i < j$ given by

$$K(\omega_{ij}) = \frac{1}{2}\,\delta_{\omega_{ij},\bar{\omega}} + \frac{1}{2}\,\delta_{\omega_{ij},-\bar{\omega}} \tag{2}$$

for some $\bar{\omega} \in [0, 2\pi)$. A more general treatment is straightforward provided that the detailed balance condition is met. For each spin in the system we assign a local neighborhood, i.e. a set of sites to which the spin is connected. Let us for simplicity abbreviate this set using $\partial i \equiv \{\ell|(\ell, i) \in \mathcal{E}_N\}$, with $|\partial i|$ representing the size of the neighbourhood of i. Our graph is characterized by the 'degree' distribution

$$p(k) = \lim_{N\to\infty} \frac{1}{N} \sum_i \delta_{k,|\partial i|} \tag{3}$$

Moments of this distribution will be denoted $\langle k^m \rangle = \sum_{k\geq 0} p(k) k^m$. We draw graphs uniformly from the ensemble of all graphs that have this given degree distribution, i.e. we use the configuration model [17]. In the thermodynamic limit this leads to interactions on a sparse graph for which the Bethe approximation is exact.

3 Equilibrium analysis

3.1 The cavity formalism on a single instance

To evaluate thermodynamic properties and the phase diagram of this system we have two main analytic tools at hand: the replica [18] and the cavity method [10]. Both of these have been used widely in a variety of settings, both in infinite- and finite-connectivity systems. Although the underlying philosophy of the two methods is different they deliver identical results. In this paper we will choose to follow the cavity method as developed for real-valued variables in [11].

The starting point of this method is to consider the marginal probability of finding a spin at site i in state ϕ_i. This follows from

$$P(\phi_i) = \frac{1}{Z_i} \int \mathrm{d}\phi_{\partial i} \; \mathrm{e}^{\beta \sum_{\ell \in \partial i} L_p(\cos(\phi_i - \phi_\ell - \omega_{i\ell}))} \, P^{(i)}(\phi_{\partial i}) \tag{4}$$

where Z_i is the appropriate normalisation constant. $P^{(i)}(\phi_{\partial i})$ is the joint probability of finding the neighbours of i in state $\phi_{\partial i} = (\phi_{j_1}, \ldots, \phi_{j_{|\partial i|}})$ in the absence of site i. To understand the origin of this expression we imagine an iterative process that creates an exact tree structure in which each spin is connected to k neighbours apart from the site at the top of the tree which has $k-1$ neighbours. At each step of this process we add a new spin to the system by bringing together $k-1$ independent branches and connecting the top site of each of these to the new site. Since, the $k-1$ branches influence each other only through the new site that has been added, we can view the probability $P^{(i)}(\phi_{\partial i})$ as the *a priori* probability of finding $\phi_{\partial i}$ before the addition of the new spin, whereas the Boltzmann factor accounts for the energetic cost of the merging. Since before the addition of the new site into the system, the $k-1$ branches were independent we can factorize $P^{(i)}(\phi_{\partial i})$:

$$P^{(i)}(\phi_{\partial i}) = \prod_{\ell \in \partial i} P^{(i)}(\phi_\ell) \tag{5}$$

This equation is the Bethe approximation and is exact, by construction, on trees. For random graph structures where loops, although predominantly long (e.g. scaling as $\log N$ on Erdös-Reyni random graphs), do exist, (5) is *approximately* correct.

Equation (4) is not closed as it relates the *true* probability distribution with the *cavity* probability distribution. To close it we simply remove a neighbour of i which

leads to

$$P^{(j)}(\phi_i) = \frac{1}{Z_i^{(j)}} \int \mathrm{d}\phi_{\partial i \setminus j} \; \mathrm{e}^{\beta \sum_{\ell \in \partial i \setminus j} L_p(\cos(\phi_i - \phi_\ell - \omega_{i\ell}))} \prod_{\ell \in \partial i \setminus j} P^{(i)}(\phi_\ell) \tag{6}$$

The two types of distributions that appear above can be dealt with either (i) by an explicit parametrization, namely setting $P^{(j)}(\phi_i) \to P(\phi_i|\{\mu_i^{(j)}\})$ (and similarly for $P(\phi_i)$) where $\{\mu_i^{(j)}\}$ play the role of cavity fields [11,12] or (ii) by using a simple histogram for each of the distibutions. Note that since spins are continuous variables, we are in principle required to introduce an infinite number of cavity fields. For all practical purposes however, one truncates the number of fields, while in some cases appropriate choices for the parameterization can be made which ensure that the impact of the truncation is not significant [12]. The histogram method of course requires advanced computational power since one needs to allocate memory space for a relatively large number of bins, but this approach has the advantage of working directly with the distributions.

Once the stationary values of (6) are known for all $i = 1, \ldots, N$ and $j \in \partial i$ we can evaluate the true probability function (4) and subsequently observables in the system, e.g. the 'magnetizations'

$$\begin{pmatrix} m_c \\ m_s \end{pmatrix} = \lim_{N\to\infty} \frac{1}{N} \sum_i \int \mathrm{d}\phi_i \; P(\phi_i) \begin{pmatrix} \cos(\phi_i) \\ \sin(\phi_i) \end{pmatrix} \tag{7}$$

and similarly for other order parameters.

3.2 The cavity formalism in the graph ensemble

To perform a bifurcation analysis of this system it is convenient to work with a graph ensemble, i.e. the set of all instance graphs $G_N = \{\mathcal{G}_N\}$ with the given degree distribution (3).

We now consider the population of the cavity probability distributions in the graph for all sites. This defines a functional density in the following way

$$W[\{P\}] = \lim_{N\to\infty} \frac{1}{N} \sum_i \frac{1}{|\partial i|} \sum_{j \in \partial i} \delta_{(F)} \left[P(\phi) - P_i^{(j)}(\phi) \right] \tag{8}$$

where by $\delta_{(F)}$ we mean a functional delta distribution in the sense that $w[f] =$

$\int dg\, w[g]\, \delta_{(F)}[g(x)-f(x)]$. Similarly, for the density of true probability distributions

$$W_{\rm true}[\{P\}] = \lim_{N\to\infty} \frac{1}{N} \sum_i \delta_{(F)}\left[P(\phi) - P_i(\phi)\right] \tag{9}$$

We can now convert (4) and (6) into self-consistent equations for (8) and (9) for the ensemble of graphs with degree distribution $p(k)$

$$\begin{aligned} W[\{P\}] = & \sum_{k\geq 0} \frac{p(k)k}{\langle k\rangle} \int \prod_{\ell=1}^{k-1} [\{\, {\rm d}P_\ell\} W[\{P_\ell\}]\ {\rm d}\omega_\ell\, K(\omega_\ell)] \\ & \times\ \delta_{(F)}\left[P(\psi) - \frac{1}{\mathcal{Z}} \prod_{\ell=1}^{k-1} \int {\rm d}\psi'\ P_\ell(\psi')\ \ {\rm e}^{\beta J L_p(\cos(\psi-\psi'-\omega_\ell))}\right] \end{aligned} \tag{10}$$

where $\mathcal{Z}$ is the appropriate normalization constant. The prefactor $p(k)k/\langle k\rangle$ expresses the fact that the probability that any given site is chosen to become a cavity site is proportional to the number of bonds it has. For the density of true probability distributions we have

$$\begin{aligned} W_{\rm true}[\{P\}] = & \sum_{k\geq 0} p(k) \int \prod_{\ell=1}^{k} [\{\, {\rm d}P_\ell\} W[\{P_\ell\}]\ {\rm d}\omega_\ell\, K(\omega_\ell)] \\ & \times\ \delta_{(F)}\left[P(\psi) - \frac{1}{\mathcal{Z}_{\rm true}} \prod_{\ell=1}^{k} \int {\rm d}\psi'\ P_\ell(\psi')\ \ {\rm e}^{\beta J L_p(\cos(\psi-\psi'-\omega_\ell))}\right] \end{aligned} \tag{11}$$

Notice that so far we did not need to make a choice for the order of the Legendre polynomial. One special case of the above equations is in the absence of angular disorder and for a fixed degree distribution $p_k = \delta_{k,c}$ and $K(\omega) = \delta(\omega)$. In this case we have a c-regular graph in which virtually every spin is living in an identical environment and one solution of (11) is $W[\{P\}] = \delta[P(\phi) - P_\star(\phi)]$ for some $P_\star(\phi)$. In the case where the order of the Legendre polynomial is $p = 1$, so that $L_1(x) = x$ and the degree distribution is Poisson, our equations reduce identically to those of [12] derived via the replica formalism.

Equation (11) can be solved in a spirit similar to the 'population dynamics' method [10,12]. As discussed in the previous section, since $W[\{P\}]$ is a measure over distributions we can encode each of these distributions using a simple histogram. Once a stationary solution for the $W[\{P\}]$ has been obtained one can proceed to evaluate observables. For example, observables describing magnetization and spin-glass order respectively follow from

$$m_c^{(k)} = \int \{\,\mathrm{d}F\} W_{\rm true}[\{P\}] \int \mathrm{d}\phi P(\phi)\cos(k\phi) \tag{12}$$

$$q_c^{(k)} = \int \{\,\mathrm{d}F\} W_{\rm true}[\{P\}] \left[\int \mathrm{d}\phi P(\phi)\cos(k\phi)\right]^2 \tag{13}$$

The order parameters (12,13) have the physical meaning

$$m_c^{(k)} = \lim_{N\to\infty} \frac{1}{N} \sum_i \overline{\langle \cos(k\phi_i)\rangle_{eq}} \tag{14}$$

$$q_c^{(k)} = \lim_{N\to\infty} \frac{1}{N} \sum_i \overline{\langle \cos(k\phi_i)\rangle_{eq}^2} \tag{15}$$

where $\langle\cdots\rangle_{eq}$ denotes thermal averages (similarly for $m_s^{(k)}$ and $q_s^{(k)}$ as averages over $\sin(\phi)$). Generally, the relevant set of observables depends (among other factors) on the particular value of p. This is accounted by the dependence of the above on the variable $k = 1, \ldots, p$. One can combine the above observables into a single pair e.g. via

$$m^{(k)} = \sqrt{(m_c^{(k)})^2 + (m_s^{(k)})^2} \quad q^{(k)} = \frac{1}{2}(q_c^{(k)} + q_s^{(k)}) \tag{16}$$

For even values of p there is no net magnetization in the system, i.e. $m^{(1)} = 0$, since the Hamiltonian is then rotationally invariant via a uniform rotation of all spins through π.

3.3 Bifurcation analysis

To perform a bifurcation analysis, we notice that $W[\{P\}] = \delta_{(F)}\left[P(\phi) - \frac{1}{2\pi}\right]$ satisfies (11) for all temperatures. Thus, we can associate this state with the high-temperature paramagnetic one (P). If one assumes that bifurcations away from this solution occur in a continuous fashion, then we can apply the so-called Guzai expansion [12], i.e. consider the perturbation $P(\phi) \to \frac{1}{2\pi} + \Delta(\phi)$, with $\int \mathrm{d}\phi\Delta(\phi) = 0$ due to normalization. A linear stability analysis then produces the following two conditions where, respectively, the first and second moments of $W[\{P\}]$ bifurcate:

$$1 = \frac{\langle k^2\rangle - \langle k\rangle}{\langle k\rangle} \max_{\ell>0} \langle\cos(\ell\omega)\rangle_\omega \frac{\mathcal{F}_p^{(\ell)}}{\mathcal{F}_p^{(0)}} \tag{17}$$

$$1 = \frac{\langle k^2\rangle - \langle k\rangle}{\langle k\rangle} \max_{\ell'>0} \frac{(\mathcal{F}_p^{(\ell')})^2}{(\mathcal{F}_p^{(0)})^2} \tag{18}$$

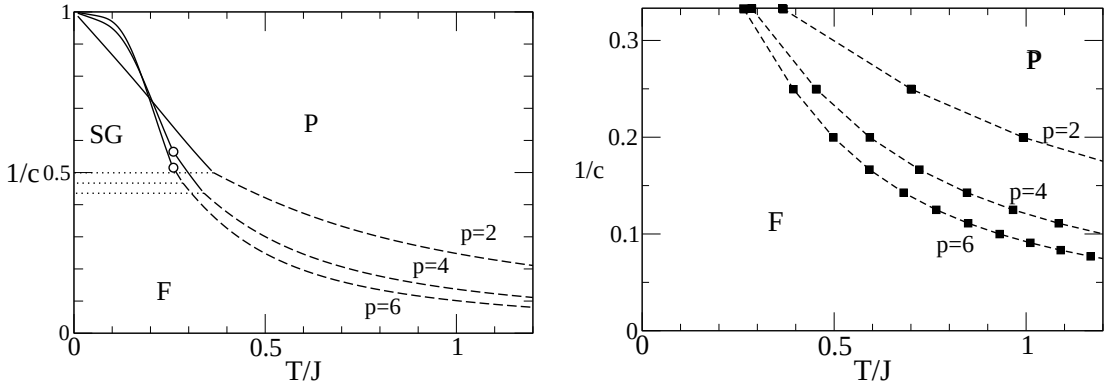


Fig. 1. Phase diagrams of the model (1) for $\bar{\omega} = \pi/8$ and for different values of p. Left figure: Poisson graph with $p(k) = e^{-c}c^k/k!$. Dashed, solid and dotted lines represent the P→F, P→SG and F→SG transition, respectively. Open circles indicate a change in the bifurcating mode. All transitions are second-order. Right figure: c-regular graph; markers correspond to integer values of c and lines are guide to the eye. For $c = 3$ and $p = 4, 6$ the transition is from P→SG.

where

$$\mathcal{F}_p^{(\ell)} \equiv \int_0^{2\pi} \mathrm{d}\phi \, \cos(\ell\phi) \;\; \mathrm{e}^{\beta J L_p(\cos\phi)} \tag{19}$$

(details on similar calculations can be found in [12]). These two conditions provide the critical temperatures where a ferromagnetic (F) and a spin-glass phase (SG) appear, respectively. The range of integers over which we maximize (17,18) expresses physically the fact that at the moment of bifurcation towards an ordered phase the distribution of spin orientations has ℓ maxima (in fact possible bifurcating modes occur at the Fourier modes $\cos(\ell\phi)$). For $p = 2$ we find that the bifurcating mode is given by $\ell = 2$ implying that spins can be ordered in a parallel or in an anti-parallel fashion (they are energetically equivalent). For larger values of p we find a transition in which the bifurcation mode changes from $\ell = 2$ to $\ell = p$.

Let us now describe the resulting phase diagrams in more detail. For $\bar{\omega} = 0$ one finds a phase diagram with a P→F transition only, while for $\bar{\omega} > 0$ richer phase diagrams occur. In figure 1 we plot phase diagrams for $\bar{\omega} = \pi/8$ for different values of p. The left picture corresponds to Poisson degree distributions $p(k) = e^{-c}c^k/k!$, while in the right picture we show the phase diagram for a regular graph. Larger values of p produce sharper P→F and P→SG transitions. The critical temperatures provided by simulation experiments and the numerical solution of our equations (16) are in good agreement with the results of the bifurcation analysis supporting the fact that all transitions are second-order (at least for $p \leq 6$ where we have currently focused). For the F→SG transition we have assumed that it is given by the dotted line. This follows from physical reasoning (absence of re-entrance

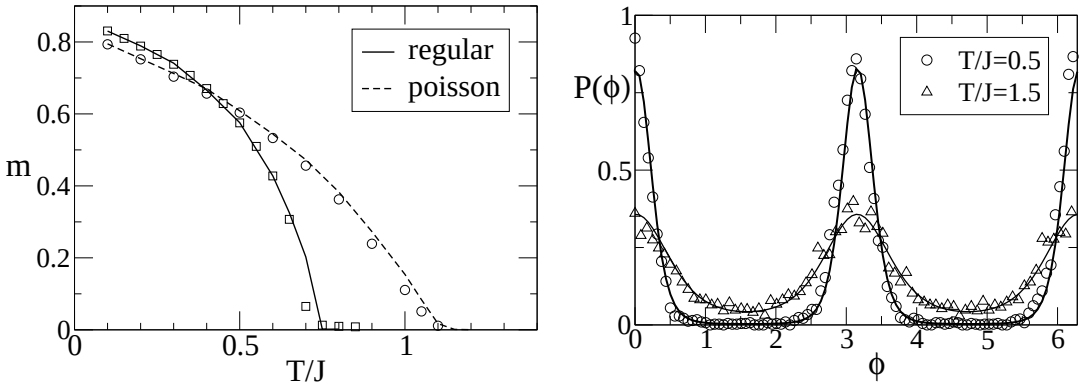


Fig. 2. Left: The order parameter $m^{(2)}$ (16) for the $p = 2$ model with $\bar{\omega} = \pi/8$ and for a Poisson- (dashed) and a regular graph (solid) with $\langle k \rangle = 4$. The critical temperatures agree well with the results of the bifurcation analysis. Right: The distribution of rod orientations $P(\phi)$ for $p = 2$. We observe two peaks at $\phi = 0, \pi$ reflecting the energetic equivalence of parallel and anti-parallel alignment. Markers in both pictures correspond to simulation experiments.

phenomena [19]). The change in the bifurcation mode is given by the open circles, namely for $T < T_{\rm circle}$ we find that $\ell = 2$ solves the maximization problem in (17,18), whereas for $T > T_{\rm circle}$ we have $\ell = p$. In the left picture of figure 2 we show the magnetization order parameter $m^{(2)}$ (16) for Poisson and regular random graphs of mean connectivity 4. In the Poisson graph transitions are smoother due to the variable number of connections per site. Markers correspond to simulation experiments of $N = 25,000$. In the right picture we show the predicted distribution of rod orientations $\mathcal{P}(\phi) = \int \{dP\} W_{\rm true}[\{P\}] P(\phi)$ against simulation experiments with $\mathcal{P}(\phi) = \frac{1}{N} \sum_i \langle \delta[\phi - \phi_i] \rangle_{eq}$ for a $p = 2$ model on a Poisson graph with $\langle k \rangle = 5$, $\bar{\omega} = 0$ and $T = 0.5$ and $T = 1.5$. We observe that $P(\phi)$ has two peaks separated by π which reflects the fact that parallel and antiparallel orientations are equivalent. Note that we have given an (arbitrary) overall rotation to the spins so that the peaks of the distribution are aligned at 0 and π. Lower temperatures promote order and as a result $P(\phi)$ is sharper for $T/J = 0.5$ than for $T/J = 1.5$.

Finally, in figure 3 we show the magnetizations $m^{(2)}$, $m^{(4)}$ and $m^{(6)}$ for a system on a regular lattice with $\bar{\omega} = 0$. Here we have chosen $p = 6$ to examine the impact of choosing a high-order Legendre polynomial. We observe that at the critical temperature $T^{(1)}_{\rm crit} \approx 1.16$ the magnetisation $m^{(6)}$ becomes non-zero; while the other two magnetisation order parameters remain zero. This bifurcation occurs at the point predicted by (17) which indicates that despite the high p-value the transition is continuous. It is interesting to note that the magnetisations $m^{(2)}$ and $m^{(4)}$ do not bifurcate until a lower temperature $T^{(2)}_{\rm crit} \approx 1.04$ is reached. This transition appears

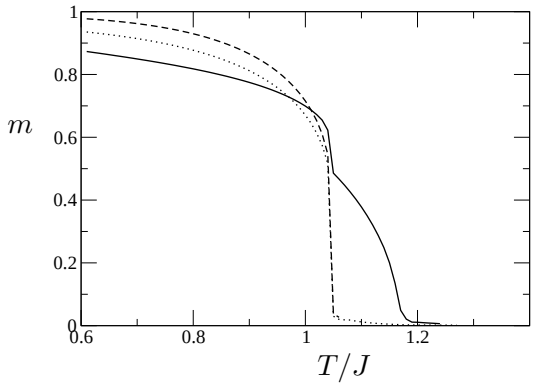


Fig. 3. The magnetisations $m^{(2)}$ (dashed), $m^{(4)}$ (dotted) and $m^{(6)}$ (solid), given by equation (16), for a system described by a Legendre order $p = 6$ on a regular lattice and with $\bar{\omega} = 0$. We see that there are two critical temperatures in this system. At the first one $T^{(1)}_{\rm crit} \approx 1.16$, which agrees with the prediction of (17), only $m^{(6)}$ becomes non-zero. For temperature values $T < T^{(2)}_{\rm crit} \approx 1.04$ the magnetisations $m^{(2)}$ and $m^{(4)}$ also become non-zero. This latter transition appears to be discontinuous.

to be discontinuous and, as it is preceded by the transition at $T^{(1)}_{\rm crit}$, we have been unable to derive it analytically (since in the ordered phase we are required to find the distribution $P(\phi)$ numerically). For temperature values between the two critical ones the ferromagnetic phase describes a system with 'local' order, i.e. relative only to the bifurcating mode (here, the sixth Fourier mode (17)).

4 Dynamics

We now turn to the relaxational dynamics of our system. The microscopic dynamics of our model is dictated by the Langevin equation

$$\frac{\mathrm{d}}{\mathrm{d}t}\phi_i(t) = -\frac{\partial H(\boldsymbol{\phi})}{\partial \phi_i} + \eta_i(t) \tag{20}$$

where $\eta_i(t)$ represents Gaussian white noise $\langle \eta_i(t) \rangle = 0$ and $\langle \eta_i(t)\eta_j(t') \rangle = 2T\delta_{ij}\delta(t-t')$. Defining the microscopic state probability $p_t(\boldsymbol{\phi}) = \langle \delta(\boldsymbol{\phi} - \boldsymbol{\phi}(t)) \rangle$ (where $\langle \cdots \rangle$ represents average over the stochastic process) we can obtain from (20) the corre-

sponding Fokker-Planck equation

$$\frac{\mathrm{d}}{\mathrm{d}t}p_t(\boldsymbol{\phi}) = \sum_{i=1}^{N}\frac{\partial}{\partial\phi_i}\left[p_t(\boldsymbol{\phi})\frac{\partial H(\boldsymbol{\phi})}{\partial\phi_i}\right] + T\sum_{i=1}^{N}\frac{\partial^2}{\partial\phi_i^2}p_t(\boldsymbol{\phi}) \tag{21}$$

We now consider a set of ℓ macroscopic observables which we denote collectively as $\boldsymbol{\Omega}(\boldsymbol{\phi}) = (\Omega_1(\boldsymbol{\phi}), \ldots, \Omega_\ell(\boldsymbol{\phi}))$ and we define accordingly the macroscopic probability distribution for these observables:

$$\mathcal{P}_t(\boldsymbol{\Omega}) = \int \mathrm{d}\boldsymbol{\phi}\, p_t(\boldsymbol{\phi})\,\delta[\boldsymbol{\Omega} - \boldsymbol{\Omega}(\boldsymbol{\phi})] \tag{22}$$

From (21) one can derive, through integration by-parts, a Fokker-Planck equation for $\mathcal{P}_t(\boldsymbol{\Omega})$

$$\begin{aligned}\frac{\mathrm{d}}{\mathrm{d}t}\mathcal{P}_t(\boldsymbol{\Omega}) = &-\sum_{k=1}^{\ell}\frac{\partial}{\partial\Omega_k}\left[\mathcal{P}_t(\boldsymbol{\Omega})\left\langle\sum_i\frac{\partial H}{\partial\phi_i}\frac{\partial\Omega_k}{\partial\phi_i} - T\frac{\partial^2\Omega_k}{\partial\phi_i^2}\right\rangle_{\boldsymbol{\Omega},t}\right]\\ &+T\sum_{h,k=1}^{\ell}\frac{\partial^2}{\partial\Omega_h\partial\Omega_k}\left[\mathcal{P}_t(\boldsymbol{\Omega})\left\langle\sum_i\frac{\partial\Omega_h}{\partial\phi_i}\frac{\partial\Omega_k}{\partial\phi_i}\right\rangle_{\boldsymbol{\Omega},t}\right]\end{aligned} \tag{23}$$

which is expressed in terms of the so-called subshell averages

$$\langle[\cdots]\rangle_{\boldsymbol{\Omega},t} \equiv \frac{\int \mathrm{d}\boldsymbol{\phi}\, p_t(\boldsymbol{\phi})\,\delta[\boldsymbol{\Omega} - \boldsymbol{\Omega}(\boldsymbol{\phi})]\,[\cdots]}{\int \mathrm{d}\boldsymbol{\phi}\, p_t(\boldsymbol{\phi})\,\delta[\boldsymbol{\Omega} - \boldsymbol{\Omega}(\boldsymbol{\phi})]} \tag{24}$$

Using (23) we obtain the evolution equations for the macroscopic observables. Let us denote $\Omega_k(t) = \int \mathrm{d}\boldsymbol{\Omega}\,\mathcal{P}_t(\boldsymbol{\Omega})\,\Omega_k$. Then integration of (23) gives

$$\frac{\mathrm{d}}{\mathrm{d}t}\Omega_k(t) = \sum_i\left\langle\frac{\partial H}{\partial\phi_i}\frac{\partial\Omega_k}{\partial\phi_i} - T\frac{\partial^2\Omega_k}{\partial\phi_i^2}\right\rangle_{\boldsymbol{\Omega}_t,t} \tag{25}$$

(assuming that the relevant boundary terms vanish) with the notation $\langle[\cdots]\rangle_{\boldsymbol{\Omega}_t,t} = \int d\boldsymbol{\Omega}\, p_t(\boldsymbol{\Omega})\,\langle[\cdots]\rangle_{\boldsymbol{\Omega},t}$. Note that (25) while exact (for reasonable choices of $\boldsymbol{\Omega}$) is not closed as it still depends on the microscopic probability $p_t(\boldsymbol{\phi})$. To eliminate this dependence we now make the equipartitioning assumption which underlies dynamical replica theory [16]: we assume that $p_t(\boldsymbol{\phi})$ depends on $\boldsymbol{\phi}$ only through $\boldsymbol{\Omega}(\boldsymbol{\phi})$ so that $p_t(\boldsymbol{\phi})$ can be removed completely from the subshell average (i.e. all microstates which give the same value of the macroscopic observables are equally likely).

Let us now be more specific and choose as our observables the magnetization and energy

$$m_c^{(k)} = \frac{1}{N}\sum_i \cos(k\phi_i) \qquad e = -\frac{J}{N}\sum_{(i,j)\in\mathcal{G}} L_p\left(\cos(\phi_i - \phi_j - \omega_{ij})\right) \tag{26}$$

$$m_s^{(k)} = \frac{1}{N}\sum_i \sin(k\phi_i) \tag{27}$$

For notational convenience we will from now suppress the time dependence in the above i.e. we will write $m_{c,t}^{(k)} \to m_c^{(k)}$ and similarly for the other observables. Calculating the various derivatives in (25) and inserting into the equations the joint spin-field distribution

$$\begin{aligned} &D_{m_c^{(k)},m_s^{(k)},e}(h,\phi) = \\ &= \frac{1}{N}\left\langle \sum_i \delta\left[h - \sum_{\ell\in\partial i}\sin(\phi-\phi_\ell-\omega_{i\ell})\frac{\partial L_p(x)}{\partial x}\right]\delta(\phi-\phi_i)\right\rangle_{m_c^{(k)},m_s^{(k)},e,t} \end{aligned} \tag{28}$$

results in the trio of ordinary differential equations

$$\frac{\mathrm{d}}{\mathrm{d}t}m_c^{(k)} = Tk^2 m_c^{(k)} - Jk\int \mathrm{d}h\,\mathrm{d}\phi\, D_{m_c^{(k)},m_s^{(k)},e}(h,\phi)\, h\sin(k\phi) \tag{29}$$

$$\frac{\mathrm{d}}{\mathrm{d}t}m_s^{(k)} = Tk^2 m_s^{(k)} - Jk\int \mathrm{d}h\,\mathrm{d}\phi\, D_{m_c^{(k)},m_s^{(k)},e}(h,\phi)\, h\cos(k\phi) \tag{30}$$

$$\frac{\mathrm{d}}{\mathrm{d}t}e = -2Te + J\int \mathrm{d}h\,\mathrm{d}\phi\, D_{m_c^{(k)},m_s^{(k)},e}(h,\phi)\, h \tag{31}$$

The distribution $D_{m_c^{(k)},m_s^{(k)},e}(h,\phi)$ represents the distribution of spins and local fields in the *microcanonical* ensemble for a given value of the magnetization and energy. Once we know this at time step t we can predict the values of the observables at time step $t+\Delta t$. To calculate this joint distribution our strategy will be to associate it to a quantity with the same physical meaning but in another physical setting [14]: we consider a *canonical* ensemble where the temperature and external fields will force the system to have the values $m_{c/s,t}^{(k)}$ and e_t. In this new system the Boltzmann distribution is given by

$$P(\boldsymbol{\phi}) = \frac{1}{\mathcal{Z}(\gamma,\{h_c^{(k)},h_s^{(k)}\})}\,\mathrm{e}^{-\gamma H(\boldsymbol{\sigma})-\gamma\sum_{k\geq 1}[h_c^{(k)}\sum_i\cos(k\phi_i)+h_s^{(k)}\sum_i\sin(k\phi_i)]} \tag{32}$$

while the joint spin-field distribution can be defined as

$$\mathcal{D}(h_i,\phi_i) = \int \mathrm{d}\phi_{\partial i}\, Q(\phi_i,\phi_{\partial i})\,\delta\left[h_i - \sum_{\ell\in\partial i}\sin(\phi_i-\phi_\ell-\omega_{i\ell})\frac{\partial L_p(x)}{\partial x}\right] \tag{33}$$

where $Q(\phi_i, \phi_{\partial i})$ represents the joint distribution of finding spin i and its neighbours in the given state. Using the reasoning that follows equation (4) and the Bethe approximation (5) we can write for tree-like structures

$$Q(\phi_i, \phi_{\partial i}) \sim \mathrm{e}^{\gamma \sum_{k\geq 1}[h_c^{(k)} \cos(k\phi_i) + h_s^{(k)} \sin(k\phi_i)] + \gamma J \sum_{\ell \in \partial i} L_p(\cos(\phi_i - \phi_j - \omega_{i\ell}))} \prod_{\ell \in \partial i} P^{(i)}(\phi_\ell) \tag{34}$$

with $P^{(j)}(\phi_i)$, as before, representing the cavity distribution of finding spin i in ϕ_i in the absence of site j and in the symbol $\sim$ we have absorbed the normalization. From here, integration with respect to the spin variables of the neighborhood of i gives the marginal distribution

$$P(\phi_i) \sim \mathrm{e}^{\gamma \sum_{k\geq 1}[h_c^{(k)} \cos(k\phi_i) + h_s^{(k)} \sin(k\phi_i)]} \int \mathrm{d}\phi_{\partial i}\, \mathrm{e}^{\gamma J \sum_{\ell \in \partial i} L_p(\cos(\phi_i - \phi_j - \omega_{i\ell}))} \prod_{\ell \in \partial i} P^{(i)}(\phi_\ell) \tag{35}$$

and removing a neighbour of i closes this to

$$\begin{aligned} P^{(j)}(\phi_i) \sim\, & \mathrm{e}^{\gamma \sum_{k\geq 1}[h_c^{(k)} \cos(k\phi_i) + \gamma h_s^{(k)} \sin(k\phi_i)]} \\ & \times \int \mathrm{d}\phi_{\partial i \setminus j}\, \mathrm{e}^{\gamma J \sum_{\ell \in \partial i \setminus j} L_p(\cos(\phi_i - \phi_j - \omega_{i\ell}))} \prod_{\ell \in \partial i \setminus j} P^{(i)}(\phi_\ell) \end{aligned} \tag{36}$$

Observables in this canonical ensemble are given by

$$\mu_c^{(k)} = \lim_{N\to\infty} \frac{1}{N} \sum_i \int \mathrm{d}\phi\ P(\phi_i) \cos(k\phi_i) \tag{37}$$

$$\mu_s^{(k)} = \lim_{N\to\infty} \frac{1}{N} \sum_i \int \mathrm{d}\phi\ P(\phi_i) \sin(k\phi_i) \tag{38}$$

$$\epsilon = -\lim_{N\to\infty} \frac{J}{N} \sum_{(i,j)\in\mathcal{G}_N} \langle L_p(\cos(\phi_i - \phi_j - \omega_{ij}))\rangle_\star \tag{39}$$

with the short-hand notation

$$\langle \cdots \rangle_\star = \frac{\int \mathrm{d}\phi_i\, \mathrm{d}\phi_j\, P^{(i)}(\phi_j) P^{(j)}(\phi_i)\ \mathrm{e}^{\gamma J L_p(\cos(\phi - \phi_j - \omega_{ij}))} [\cdots]}{\int \mathrm{d}\phi_i\, \mathrm{d}\phi_j\, P^{(i)}(\phi_j) P^{(j)}(\phi_i)\ \mathrm{e}^{\gamma J L_p(\cos(\phi_i - \phi_j - \omega_{ij}))}} \tag{40}$$

The above equations can be easily re-written in a graph-ensemble form for a given degree distribution.

We see that this is now equivalent to an equivalent static calculation (using a more involved Hamiltonian): at each time step t and given the values of observables

$m^{(k)}_{c/s,t}$ and e_t, one has to find the values of the temperature γ and external fields $h^{(k)}_c, h^{(k)}_s$ that via the definitions (37), (38) and (39) ensure that the equalities $\mu^{(k)}_c = m^{(k)}_{c,t}$, $\mu^{(k)}_s = m^{(k)}_{s,t}$, $\epsilon = e_t$ are satisfied. Once the correct values of the parameters have been found one can evaluate the joint spin-field distribution (33) and this corresponds to $D_{m^{(k)}_c, m^{(k)}_s, e}(h, \phi)$.

While the conceptual formulation of this methodology is relatively straightforward, the numerical implementation is a bit more challenging. For each time step, one has to solve the inverse problem of finding the correct values of the temperature γ and external fields $h^{(k)}_c, h^{(k)}_s$ which produce a given magnetization and energy. Thus the search space is already $(2k+1)$-dimensional and computational costs are not negligible. The algorithm also requires the convergence of population dynamics and we are thus required to work in regions of phase space where only trivial ergodicity breaking occurs. For these reasons we have implemented our algorithm in the simple scenario of $p = 2$ (in which case $m^{(1)} = 0$) which allows us to restrict the present set of observables to $(m^{(2)}_c, m^{(2)}_s, e)$. We have considered a 3-regular graph. The results are shown in figure 4. We see that the analytic solution compares perfectly with simulations for small and very large times, but for intermediate times the two clearly deviate. This is due to the assumptions we have made, namely equipartitioning in the space of the three observables. We expect that by choosing a larger set of macroscopic observables (e.g. incorporating correlation functions) this approximation will improve. There is also an error introduced due to the presence of loops in the graph; for smaller graphs we would expect a larger deviation due to the incorrectness of the Bethe ansatz, while in the truly infinite system these will not occur.

5 Discussion

In this paper we have studied the Lebwohl-Lasher model, which has a characteristic energy landscape of sharp and narrow wells. This model has been studied extensively in liquid crystal models and our approach here can be seen as the Bethe approximation to the finite dimensional problem. We have considered random graph lattices. At equilibrium our treatment follows the general methodology developed in [11] based on the cavity method within the ergodic (replica-symmetric) assumption. We have given bifurcation conditions describing the phase diagram. Numerical evaluation of the order parameters shows the transition from ordered to

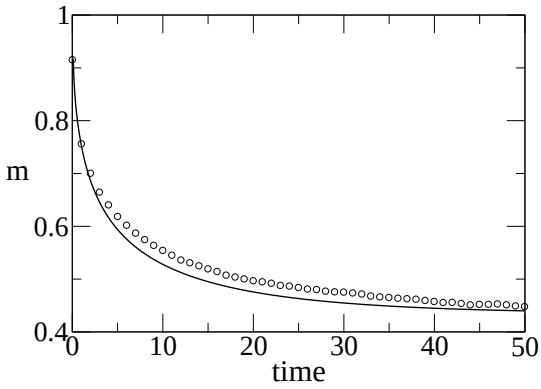


Fig. 4. The evolution of the magnetization $m^{(2)} = [m_c^{(2)} + m_s^{(2)}]^{\frac{1}{2}}$ for a 3-regular lattice and $p = 2$ from a highly ordered initial state in a heat-bath of temperature $T = 0.6$ and $\bar{\omega} = 0$. The solid line represents the theoretic prediction and markers Langevin simulations of $N = 40\,000$ spins.

paramagnetic phase. This transition, as in Ising spin systems, is sharper for regular than for random lattices. Simulation experiments are in excellent agreement with the analytic results.

We have also extended the formalism developed in [13] for the dynamics of spin systems on finitely-connected systems into situations where spins are continuous variables. Our starting point has been the Langevin equation for the microscopic dynamics from which a set of differential equations follows for our chosen set of observables. The key to solving this set of evolution equations is the approximations of dynamical replica theory [16]. We have contrasted the results of this methodology with simulation experiments. This shows that despite the appealingly clean analytic form, there are weaknesses of the formalism that need to be dealt with in the future. In particular, the assumption of equipartitioning of the microscopic state probability within the subshells is too strong for small sets of observables while for larger ones the computational costs start becoming prohibitive.

Acknowledgements

We are indebted to Isaac Pérez Castillo and Tatsuya Uezu with whom we developed the dynamics of continuous spin systems on graphs. NS wishes to thank A C D van Enter for a very motivating introduction to liquid crystal models. This paper has been prepared by the authors as a commentary on the topic as at November 2006 and is not a definitive analysis of the subject matter covered. It does not constitute advice or guidance in this area and should not be relied upon as such. The paper

has not been prepared by JH in his capacity as an employee of Hymans Robertson LLP and the views expressed do not represent those of Hymans Robertson LLP. Neither the authors nor Hymans Robertson LLP accept liability for any errors or omissions.

References

[1] A Lebwohl and G Lasher (1973) *Phys Rev A* **6** 426

[2] E Domany, M Schick and R H Swendsen (1984) *Phys Rev Lett* **52** 1535

[3] A Jonsson, P Minnhagen and M Nylén (1992) *Phys Rev Lett* **70** 1327

[4] N Priezjev and R A Pelcovits (2001) *Phys Rev E* **63** 062702

[5] B Berche and R Paredes (2005) *Cond Matt Phys* **8** 723

[6] A I Fariñas Sánchez, R Paredes and B Berche (2005) *Phys Rev E* **72** 031711

[7] J V Selinger and B R Ratna (2004) *Phys Rev E* **70** 041707

[8] Z Zhang, O G Mouritsen, and M J Zuckermann (1992) *Phys Rev Lett* **69** 2803

[9] U Fabbri and C Zannoni (1986) *Molec Phys* **58** 763

[10] M Mézard and G Parisi (2001) *Eur Phys J B* **20** 217; I Kanter and H Sompolinsky (1987) *Phys. Rev. Lett* **58** 164; M Mézard and G Parisi (1987) *Europhys. Lett* **3** 1067

[11] N S Skantzos, I Pérez Castillo and J P L Hatchett (2005) *Phys. Rev. E* **72** 066127

[12] A C C Coolen, N S Skantzos, I Pérez Castillo, C J Perez Vicente, J P L Hatchett, B Wemmenhove, T Nikoletopoulos (2005) *J Phys A* **38** 8289-8317

[13] J P L Hatchett, I Pérez Castillo, A C C Coolen and N S Skantzos (2005) *Phys Rev Lett* **95** 117204

[14] G Semerjian and M Weigt (2004) *J Phys A* **37** 5525

[15] H Hansen-Goos and M Weigt (2005) *J Stat Mech: Theory & Experiment* P08001

[16] A C C Coolen, S N Laughton, D Sherrington (1996) *Phys Rev B* **53** 8184; S N Laughton, A C C Coolen, D Sherrington (1996) *J Phys A* **29** 763; A C C Coolen and D Sherrington (1993) *Phys Rev Lett* **71** 3886

[17] M Molloy and B Reed (1995) *Random Structures & Algorithms* **6** 161–179

[18] M Mezard, G Parisi, and M A Virasoro (1987) 'Spin glass theory and beyond', World Scientific Publishing Co.

[19] G Parisi and G Toulouse (1980) *J Phys Lett (Paris)* **41** L361